Polymer 50 (2009) 6287–6296

Contents lists available at ScienceDirect

Polymer

journal homepage: www.elsevier.com/locate/polymer

Effect of uniaxial drawing on the structure and glass transition behavior of poly(trimethylene 2,6-naphthalate)/layered clay nanocomposites

Ahmad Nawaz Khan [a], Po-Da Hong [a,b,*], Wei-Tsung Chuang [c,**], Kan-Shan Shih [d]

[a] Graduate Institute of Materials Science and Technology, National Taiwan University of Science and Technology, Taipei 106, Taiwan
[b] Department of Polymer Engineering, National Taiwan University of Science and Technology, Taipei 106, Taiwan
[c] National Synchrotron Radiation Research Center, Hsinchu 300, Taiwan
[d] School of Dentistry, National Defense Medical Center, Taipei 114, Taiwan

ARTICLE INFO

Article history:
Received 1 July 2009
Received in revised form
16 October 2009
Accepted 23 October 2009
Available online 30 October 2009

Keywords:
Nanocomposite
Polytrimethylene 2,6-naphthalate
Glass transition

ABSTRACT

The structure–property relationships of poly(trimethylene 2,6-naphthalate)/layered clay nanocomposites are being investigated under uniaxial drawing by using synchrotron wide angle X-ray diffraction, small angle X-ray scattering, transmission electron microscope and dynamic mechanical analyzer. The cold crystallization at 110 °C of PTN and nanocomposites samples under drawing induced the α-crystal form with the chain axis (*c*-axis) aligned along the drawing direction as well as parallel to the layered clay surface. However, the broad surfaces of the layered clay are oriented and rotated nearly perpendicular to the sample's surface, forming the house of cards type structure. Such structural formation of layered clay in the PTN matrix influenced the thermomechanical properties depending on the extent of confinement and surface interaction effects. The amorphous and crystallized structures of the nanocomposites showed the analogous tendency in which T_g decreased and increased before and after drawing, respectively, relative to the neat PTN. Despite the evolution of free volume after drawing, the nanocomposites exhibited an unusual positive shifting trend in T_g. The deviation of T_g in the PTN nanocomposites system is ascribed to the interplay of two competing effects; (i) the increase in the local free volume owing to the confining effect of intercalation (enhanced the chain mobility) and (ii) entropic constraint imposed by the stronger interfacial interaction due to the physical jamming of layered clay (retarded the chain mobility).

1. Introduction

Polymer-clay nanocomposites generate an interesting subject of research owing to their excellent improvement in the physical, mechanical and thermal properties of materials [1–6]. The enhancement of these properties depends not only on the presence of the large specific surface area of the layered clay (750 m^2/g) but also on the interaction between polymer chains and layered clay. In the recent few years, many researchers have shed a light on the glass-transition dynamics of the polymer nanocomposites [7–19], however, it challenges the common understanding that how the trace amounts of layered clay alter significantly the chain dynamics of the polymer system. The diversified change in the sign of glass-transition temperature (T_g) compared to the bulk has been observed in the polymer/nanoparticles [7–11] and polymer/layered clay nanocomposites [12–19]. Many attempts by experiments and simulations have been undertaken to explain these observations [20–23], but no universal model is available so far.

The sign of T_g shift is strongly dependent on the interface morphology, interparticle spacing and polymer–nanoparticles interactions. Arceo et al. [9] found that the controlled spatial distribution of the grafted nanoparticles have markedly dropped T_g as much as 65 °C, within a thin film polystyrene/gold nanoparticle system. The modification in T_g is also observed for the wetting and dewetting effects at the polymer–nanoparticle interface [10]. Narayanan et al. [11] suggested that the internal stress, to counter the reduction in the entropy of the polymer at the interface region, contributed to decrease T_g. Srivastava et al. [7] proposed that T_g shift under confinement is determined by a competitive balance between the interfacial width and the length of cooperatively rearranging region (CRR). On the other hand, complicated relaxation dynamics in the polymer/layered clay nanocomposites relative to the nanoparticles can be expected due to the geometrical

* Corresponding author. Department of Polymer Engineering, National Taiwan University of Science and Technology, Taipei 106, Taiwan.
** Corresponding author. Tel.: +886 2 27376539; fax: +886 2 27376544.
E-mail addresses: poda@mail.ntust.edu.tw (P.-D. Hong), weitsung@nsrrc.org.tw (W.-T. Chuang).

0032-3861/$ – see front matter © 2009 Elsevier Ltd. All rights reserved.
doi:10.1016/j.polymer.2009.10.056

constraint imposed by the two-dimensional space of the intercalated and exfoliated structures. The change in T_g is not only attributed to the extent of interaction among the polymer chains and layered clay but also to the confinement effect of the tethered chains. Thus, the interplay of the confinement and surface effects imperatively dictate a sign of T_g shift [24,25]. Both the intercalated and exfoliated structures exhibited the decrease and increase in T_g, [12–19,26–28] though Vaia et al. [29] also reported the absence of T_g in the intercalated systems.

The relaxation dynamics of the polymer chains near T_g is essentially cooperative [30] and becomes sensitive to the local environment. The faster relaxation dynamics is observed when the polymer chains are confined in a few nanometers spaces inside the clay galleries [31,32]. Moreover, the physical or chemical attachment of the polymer chains with the layered clay alters the segmental mobility due to the difference in the entanglement density and configurational entropy near the clay surface. Evidently, a strong interaction among the polymer and clay/substrate surface increases T_g, while weakly interacting surface decreases T_g [33–39].

Poly(trimethylene 2,6-naphthalate) (PTN) is a promising material for engineering thermoplastics and textile fibers. Many studies about the crystal structure, crystallization and melting behavior, polymerization kinetics, rheological and thermal properties of PTN have been reported [40–45] but this is the first contribution regarding the inclusion of layered clay in the PTN matrix. The orientation plays a key role in the processing of polymer nanocomposites. However, this is unclear so far how the orientation affects the T_g behavior of the polymer nanocomposites. In this work, we investigate the shifting trend of T_g correlated with the structural orientation under drawing and/or cold crystallization in the PTN/layered clay nanocomposites. The amorphous and crystallized structures of the PTN nanocomposites, before and after drawing, are characterized to obtain the insight into the shifting mechanism of T_g. Wide-angle X-ray diffraction (WAXD), small-angle X-ray scattering (SAXS) and transmission electron microscope (TEM) are employed to elucidate the structure of the nanocomposites. Furthermore, the length scale of cooperatively rearranging region (CRR) is used to comprehend the shift in the sign of T_g.

2. Experimental section

2.1. Materials

PTN was kindly supplied by Shell Chemical Company, having intrinsic viscosity of 0.6 dL/g measured in a mixed solution of phenol/tetrachloroethane (6/4, w/w) at 25 °C. Cloisite 93A with basal spacing of 23.6 Å was provided by Southern Clay Products [46] and used as received. The wt% of Cloisite 93A was kept 1%, 5% and 15% in the PTN matrix and termed as PTNC's in general and particularly PTNC1, PTNC5 and PTNC15 respectively.

2.2. Sample preparation

To obtain the well dispersion of Cloisite 93A in PTN matrix, the solution method was used as described in our previous paper [47]. In short, PTN and 93A were dried for 24 h at 90 °C before mixing to minimize the moisture content. The weighed amounts of 93A and PTN were dissolved in the hexafluoroisopropanol solvent and the solution was stirred and sonicated for few hours. After drying, the films were melted at 250 °C for 5 min, pressed into a rectangular shape sample with dimensions of 30 mm length, 5 mm width and 1 mm thickness between two Teflon sheets and quenched in the liquid nitrogen to obtain fully amorphous structure (named as the undrawn amorphous). The quenched samples were isothermally cold crystallized at 110 °C for 24 h in the oven and termed as the undrawn crystallized. Furthermore, the quenched samples were drawn up to 3 draw ratio at 110 °C (35 °C above T_g) as well as up to 2 draw ratio at 60 °C (15 °C below T_g) and called the drawn crystallized and the drawn amorphous, respectively. For drawing, the specimen was gripped in the portable hot drawing device (TST-350) at the rate of 300 μm/sec with pre-load of 200 N. After drawing, the increase in length was proportional to the decrease in the thickness of the specimen.

2.3. Characterization

2.3.1. X-ray measurements

WAXD and SAXS measurements were performed at beamlines BL01C (powder X-ray scattering endstation) and BL17B3 (a small angle X-ray scattering endstation) of the National Synchrotron Radiation Research Centre (NSRRC), Taiwan. In WAXD measurement, the incident beam was monochromated to 16 kev (wavelength $\lambda = 0.7749$ Å) and collimated by 30 cm collimator of 1 mm diameter. The WAXD data was collected using mar345 imaging plate detector. The scattering angle was calibrated by a mixture of silver behenate and silicon powders. The SAXS measurement was performed using $\lambda = 1.2389$ Å, SAXS area detector and the sample to detector distance of 1200 mm. The 0.5 mm diameter beam was collimated by one set of slits and two sets of Ta pinholes. All the data was corrected for electronic noise, background scattering and detector sensitivity. The wavevector transfer q ($=4\pi\sin(\theta/2)/\lambda$) defined by the scattering angle θ and λ of the X-rays was calibrated by the standard sample of silver behenate.

2.3.2. Transmission electron microscope

TEM micrographs were taken using JEOL (JEM-1400) at an accelerating voltage of 120 kV. The thin sections of about 90 nm were cut in the thickness directions (TD and DD) by using reichert

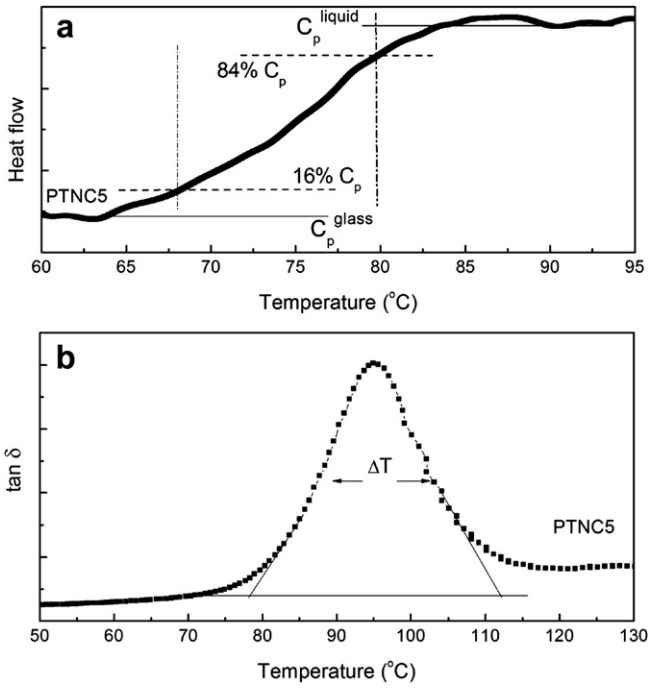

Fig. 1. (a) DSC curve to determine the specific heat capacity $(\Delta C_p)_m$ and (b) DMA spectra of tan δ curve for the determination of ΔT = full width at half maximum of the curve.

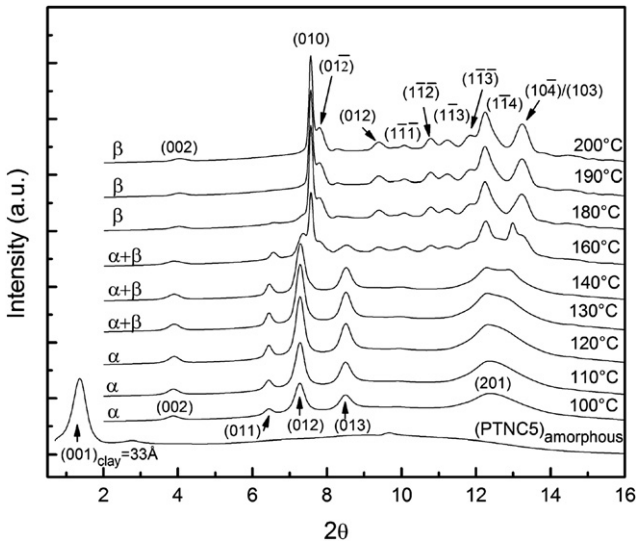

Fig. 2. WAXD profiles of PTN isothermally cold crystallized at various temperatures and amorphous structure of PTNC5 prior to drawing.

ultracut E cryomicrotome at room temperature with diamond knife and collected in the copper grid.

2.3.3. Differential scanning calorimetry

DSC was carried out in Perkin Elmer Pyris instrument, equipped with intracooler. Dry N_2 gas was purged through DSC furnace at flow rate of 30 ml/min. The mass of the sample was kept about 5 mg and heated at the rate of 2.5 °C/min. The temperature and heat flow rates were calibrated with indium and zinc standards.

2.3.4. Dynamical mechanical analyzer

DMA was performed using 01db-Metravib-DMA50N equipment in the shear mode. The samples were subjected to the frequency of 1 Hz with dynamic displacement of 50 μm and heated at the rate of 2 °C/min. T_g is observed from the peak maximum of tan δ curves and found to be about 25 °C higher than DSC data because of the different frequency of perturbation involved in their measurements [30].

2.4. Analysis of the glass transition dynamics

According to Adams-Gibbs theory, T_g has a spatial length effect which is cooperatively correlated to the segmental motion within the characteristic length of cooperativity (ξ_a) [30,48]. The finite size layer of ξ_a extends approximately to the length scale of confinement caused by the layered clay. Therefore, CRR size is calculated using the thermal fluctuation theory, proposed by Donth [49] as follows,

$$V_a = \xi_a^3 = \frac{k_\beta T_g^2}{(\Delta C_p)_m (\delta T)^2 \rho} \quad (1)$$

where V_a is the mean volume of one CRR, k_β is the Boltzmann constant, ρ is the bulk density (ca. 1.393 g/cm^3) of PTN [40], and $(\Delta C_p)_m$ is the measured heat capacity between 16% and 84% of the total ΔC_p at T_g (Fig. 1a). δT is the mean temperature fluctuation of one average CRR and determined from the temperature interval ΔT obtained from the full width at half maximum of the tan δ curves (Fig. 1b). The width of glass transition interval ΔT measured in temperature units is $\approx 2\delta T$ [49]. ξ_a is attributed to the region of minimum extent where chains must rearrange in a cooperative manner to induce mobility in the blocked chain [30]. Additionally,

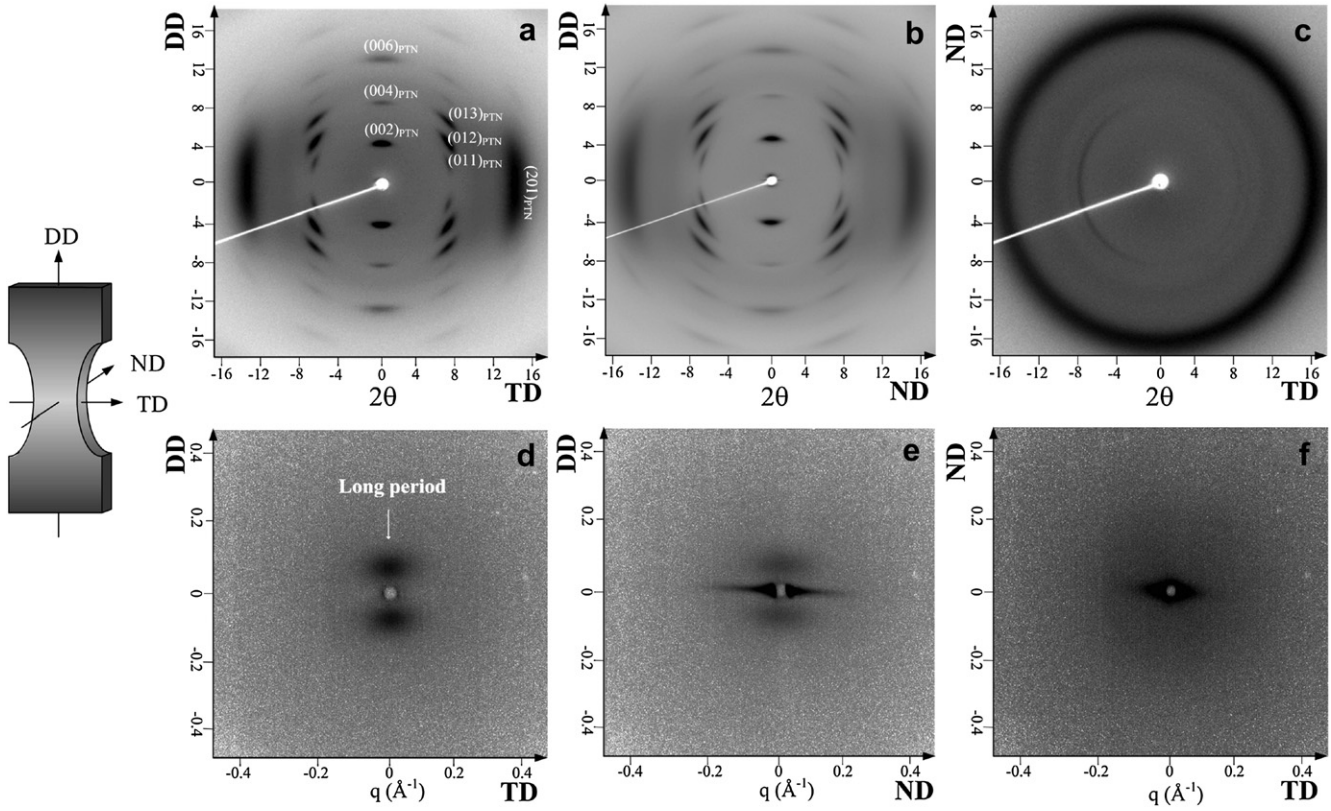

Fig. 3. Two dimensional WAXD and SAXS patterns of PTN after drawing at 110 °C along the ND (a, d), TD (b, e) and DD (c, f). The inset shows the three principal directions of the specimen with respect to the X-ray beam.

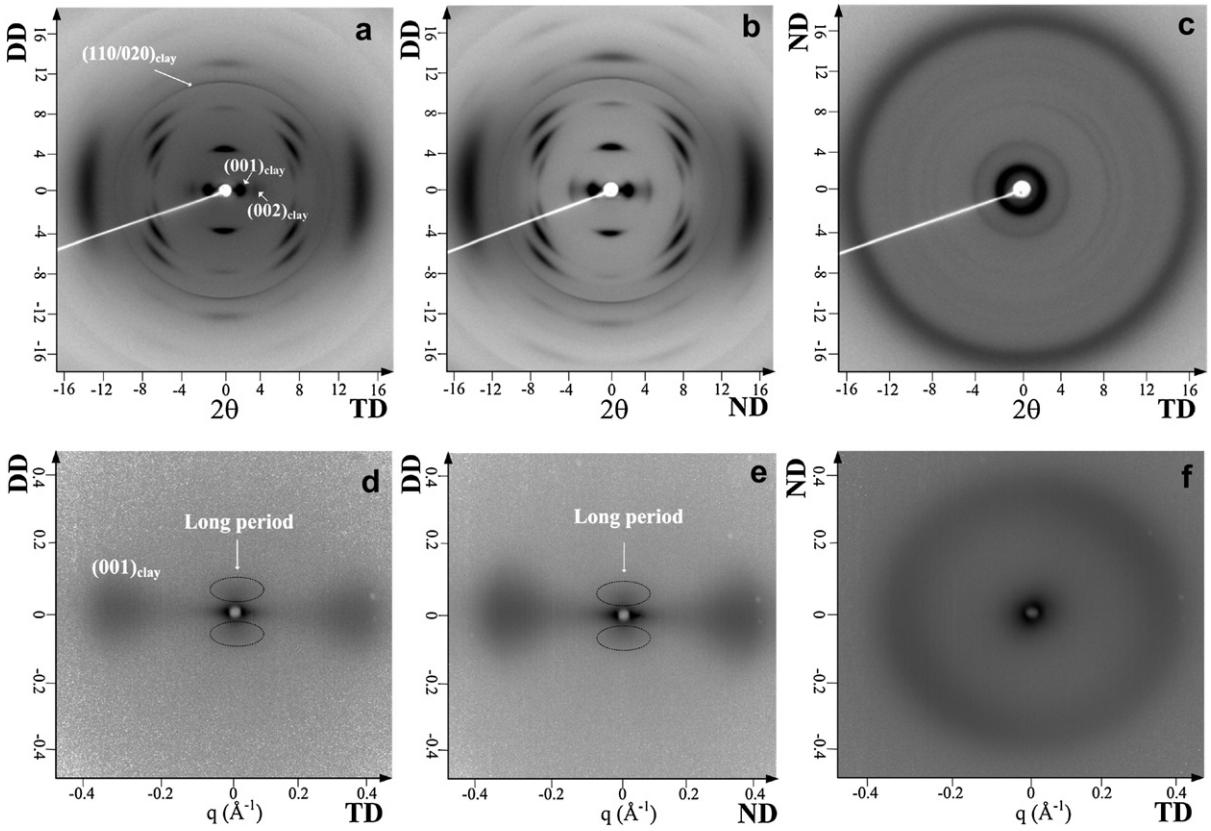

Fig. 4. Two dimensional WAXD and SAXS patterns of PTNC5 after drawing at 110 °C along the ND (a, d), TD (b, e) and DD (c, f).

the number of particles (N_{CRR}) present in one average CRR volume is calculated as follows,

$$N_{CRR} = \left(\frac{\rho V_a N_A}{M_0}\right) \quad (2)$$

where N_A is Avogadro's number and M_0 is the molecular weight of a single repeat unit of PTN. N_{CRR} involved in the cooperativity length is the necessary collection of polymer segments which must move together in a given time and space scale. T_g obtained from DMA data is relatively suitable due to the physical meaning of ξ_a because this length scale is cooperatively correlated to the dynamic mobility of the chains in the amorphous phase.

3. Results and discussions

3.1. Structural characterization of PTN and layered clay after drawing

Fig. 2 shows the WAXD profiles of cold-crystallized PTN at various isothermal temperatures (T_c). The α and β-crystals develop at T_c below 130 °C and above 170 °C, respectively; however, both crystal forms coexist between the above mentioned temperatures. The α-form with monoclinic crystal is a metastable phase, while β-form with triclinic crystal is a stable phase [41,42]. The polymorphic transition temperatures are the same in cold and melt crystallization of PTN [43]. Furthermore, the inclusion of layered clay into the PTN matrix forms the intercalated structure as revealed by the WAXD curve of the amorphous PTNC5. The insertion of PTN chains into the clay galleries enhances the basal spacing of clay (d_{001}) from 2.3 to 3.3 nm.

In order to study the preferred orientation of PTN crystal and layered clay platelets, Figs. 3 and 4 present 2D- WAXD and SAXS

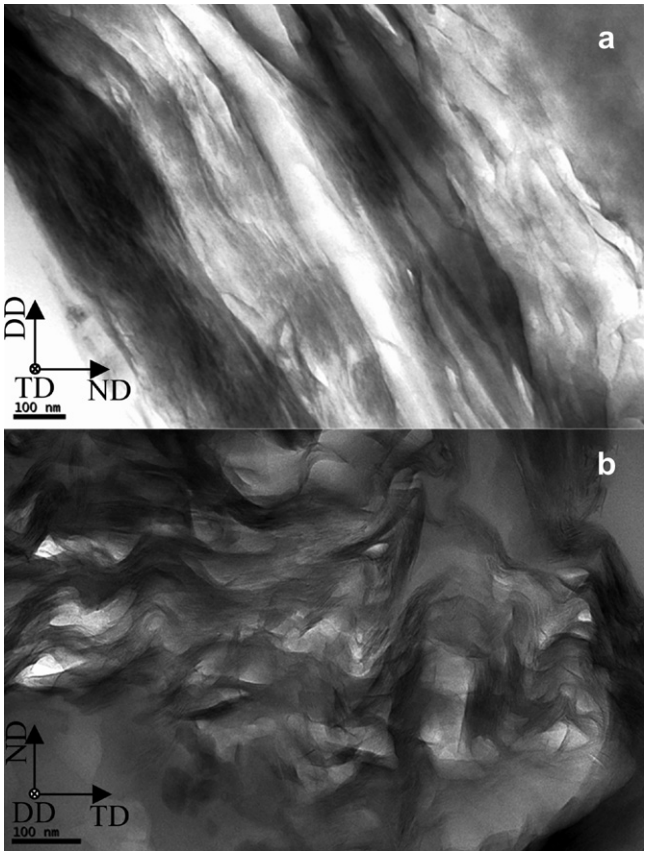

Fig. 5. TEM morphology of the drawn samples of PTNC5 along the (a) TD and (b) DD. The scale bar is 100 nm.

patterns in three directions of the sample for PTN and PTNC5, respectively. An illustration in the inset of Fig. 3 exhibits three orthogonal views of the sample with respect to the X-ray beam, where DD, ND and TD are the drawing direction, normal direction, and transverse direction, respectively. The results of PTNC1 and PTNC15 are similar to PTNC5 therefore not shown for the sake of brevity.

Considering the drawing of neat PTN, Fig. 3a and b shows the similar WAXD patterns with the incident X-ray beam along the ND and TD in which the (002), (004) and (006) reflections appear in the meridional direction and the (201) reflection displays in the equatorial direction. The WAXD pattern with the X-ray beam along the DD in Fig. 3c solely presents the isotropic ring of the (201) reflection. Notably, the angle between the normal of the (201) plane and *c*- and *b*- axes are 81.2° and 90°, respectively, in the monoclinic unit cell of the α-crystal [41,42]. These WAXD results imply that *c*-axis of the α-crystal (chain axis) is oriented parallel to the DD, while both the *a*- and *b*-axes are randomly distributed in the ND-TD plane perpendicular to the DD for strain induced cold crystallization. The semi-circle ring of the (011) reflection in Fig. 3c is due to the slight misalignment of the sample.

Fig. 3d–f shows the SAXS patterns corresponding to the WAXD patterns of Fig. 3a–c. Two scattering lobes are located with the scattering maxima in the meridional direction of the ND and TD patterns (Fig. 3d and e) but absent in the DD pattern (Fig. 3f). It indicates that the lamellar structure of the α-crystal with a long period of 11.8 nm is stacked along the drawing direction. After drawing, the long period of the α-crystal becomes thicker than that of quiescent crystallization (ca. 8 nm) [43]. In contrast to the ND pattern, the TD and DD patterns show strong equatorial streak from the beam center because of a surface scattering arisen by the long sample-path-length of thin-film edge. The absence of streak in the ND pattern ruled out the presence of Shish-Kebab structure and discerns the inducement of *c*-axis-oriented lamellae of the α-crystal in neat PTN. Recently, Kawakami et al. [50] reported that Polyethylene terephthalate (PET) also exhibited the *c*-axis orientation of lamellae after drawing under cold crystallization.

The WAXD and SAXS patterns of PTNC5 shown in Fig. 4 have the α-crystal inducement as observed in neat PTN (Fig. 3). The spots of (001) and (002) reflections near the beam stop in the equatorial direction and a sharp reflection from the (110/020) in the meridional direction of Fig. 4a (ND) and b (TD) are related to the orientation of layered clay platelets. The DD pattern in Fig. 4c displays the isotropic rings of the (001), (002) and (110/020) reflections. In the corresponding SAXS patterns of Fig. 4d (ND) and Fig. 4e (TD), the azimuth angle between the scattering lobes and the (001) reflection of clay is 90°, indicating that the lamellae stacking of the α-crystal are oriented perpendicular to the layered clay. The scattering lobes in PTNC5 shift to lower angle implying an increase in the long period up to 18.4 nm due to the heterogeneous nucleating

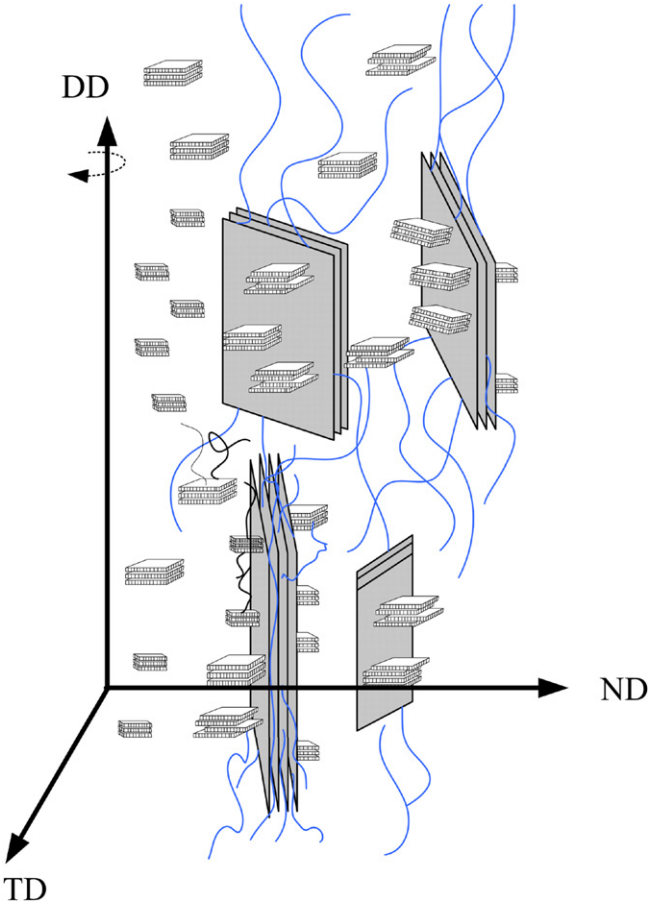

Fig. 6. The schematic illustration of the orientation of the layered clay platelets and lamellae in PTNC5 after drawing at 110 °C. (For interpretation of the references to colour in this figure legend, the reader is referred to the web version of this article.).

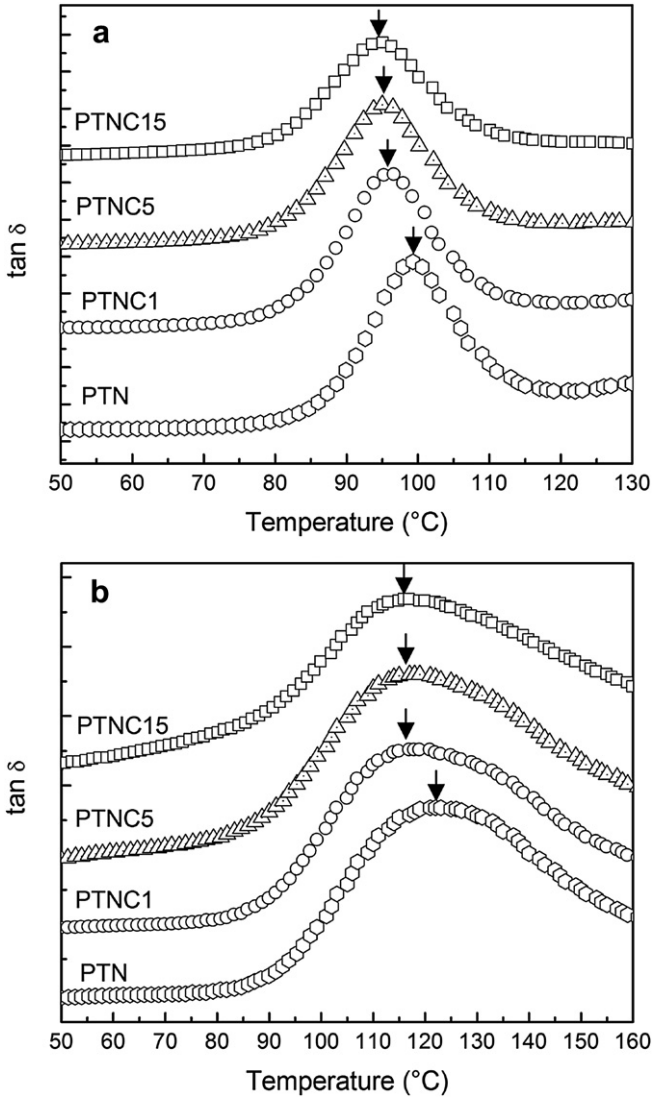

Fig. 7. The tan δ curves of the PTN and PTNC's for the (a) undrawn amorphous and (b) undrawn crystallized structures.

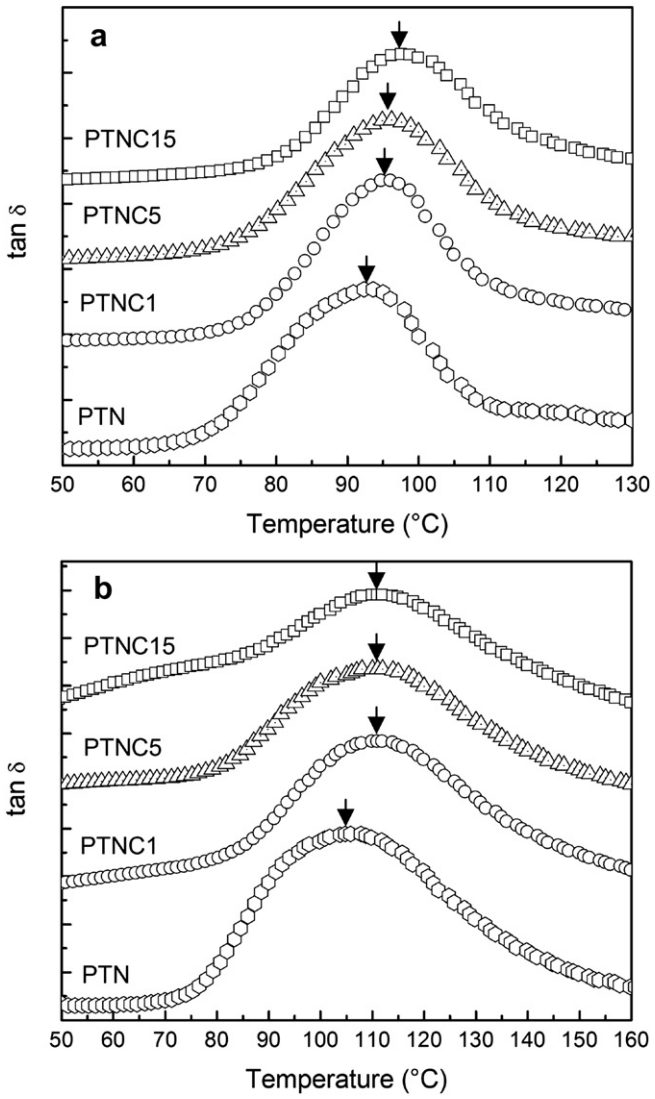

Fig. 8. The tan δ curves of the PTN and PTNC's for the (a) drawn amorphous and (b) drawn crystallized structures.

effect of layered clay in the PTN matrix. Additionally, the intercalation extent is slightly reduced to 3 nm after the crystallization. Fig. 4f (DD) shows the isotropic scattering from the (001) reflection of the clay platelets. From these WAXD and SAXS results, the random orientation of layered clay along the DD while preferential orientation in the ND and TD patterns infer that the broad surfaces of the clay platelets nearly become perpendicular to the sample's surface. Such arrangement of layered clay leads to the formation of house of cards like structure. Our results differ from the previous studies in which clay platelets were oriented parallel to the sample's surface [51–56].

The TEM micrographs of PTNC5 sectioned in the TD and DD sides are shown in Fig. 5 and manifest the intercalated structure of layered clay in the PTN matrix. Fig. 5a shows the edges of clay platelets, preferentially aligned and oriented perpendicularly in the DD-ND plane, although the faces of layered clay cannot be observed clearly in this plane. This is consistent with the finding of Okamoto et al. [57]; he found that at higher drawing ratio up to 3 ~ 4, the faces of clay in the DD-ND plane were not seen. Fig. 5b shows the random dispersion of clay layers, bent with wavy shape in the ND-TD plane owing to the breakage or buckling of the clay platelets along the DD. This is expected because the specimen under drawing becomes thinner, causes tension along and compression perpendicular to the drawing direction which in turn leads to the buckling/breakage of clay layers [54].

The structural orientation of the clay platelets and the lamellae of the α-crystal are schematically illustrated in Fig. 6 as revealed from WAXD, SAXS and TEM results. Before drawing and cold crystallization of the PTNC5 amorphous film, the clay layers were randomly oriented and PTN chains were intercalated in the clay galleries as well as surrounding the clay platelets, forming a network of PTN chains-clay platelets. In this network, PTN chains were attached or physically associated to the clay surface. When the PTNC5 film is cold crystallized under drawing, the oriented PTN chains develop the *c*-axis-lamellae due to the relaxation along longitudinal and/or transversal chain retraction [58–60]. Moreover, the *c*-axis orientation of tethered chains forces the clay platelets to align in the DD while the *c*-axis-oriented lamellae may cause rotation of the clay platelets to randomize the clay orientation. Evidently, an orientational correlation exits among the layered clay and the crystallites in which the crystallites dictate the orientation and rotation of the clay platelets as observed from the random orientation of layered clay (Fig. 4c) caused by the crystallites (Fig. 3c). Such orientational correlation exerts the rotational displacement of clay platelets around the *c*-axis and give rise to the house of cards type structure in the PTN matrix. Okamoto et al. [57] reported the house of card structure for PP/clay nanocomposites under uniaxial elongation deformation, owing to the interaction between clay layers and modified PP matrix with small amount of maleic anhydride (MA) groups. But house of card structure is never found in nylon6/clay nanocomposites because the γ-form is converted to α-form under drawing which is nucleated far from the clay, having no any orientational correlation with the clay layers [54,61].

Table 1
The values of heat capacity (ΔC_p), glass transition temperature (T_g), thermal fluctuation (ΔT), CRR size (ξ_a), number of segments in the CRR size (N_{CRR}) and intergallery spacing (d_{clay}) for undrawn amorphous and crystallized structures of PTN and PTNC's. The value of crystallinity (Xc) is also given for undrawn crystallized PTN and PTNC's determined from DSC.

Samples	Undrawn amorphous						Undrawn crystallized						X_c[d] %
	ΔC_p[a] J/g K	T_g, °C	ΔT, °C	ξ_a[b] nm	N_{CRR}[c]	d_{clay}, nm	ΔC_p[a] J/g K	T_g, °C	ΔT, °C	ξ_a[b] nm	N_{CRR}[c]	d_{clay}, nm	
PTN	0.335	99	16	4	190	–	0.12	123	45	2.9	75	–	33
PTNC1	0.255	96	15	4.5	280	3.3	0.085	118	48	3.1	90	3	33
PTNC5	0.241	95	15	4.6	290	3.3	0.07	118	50	3.2	100	3	34
PTNC15	0.223	94	15	4.7	315	3.3	0.055	118	55	3.3	110	3	35
Clay						2.3						2.3	

[a] ΔC_p is normalized for the clay content.
[b] ξ_a values are limited to one digit after the decimal place.
[c] N_{CRR} values are rounded to nearest five.
[d] Crystallinity is determined using the expression; $X_c = \Delta H/\Delta H^0(1-\Phi)$, where Φ is the wt% of layered clay.

Table 2
The values of heat capacity (ΔC_p), glass transition temperature (T_g), thermal fluctuation (ΔT), CRR size (ξ_a), number of segments in the CRR size (N_{CRR}) and intergallery spacing (d_{clay}) for drawn amorphous and crystallized structures of PTN and PTNC's. The value of crystallinity (X_c) is also given for drawn crystallized PTN and PTNC's determined from DSC.

Samples	Drawn amorphous						Drawn crystallized						X_c[d] %
	ΔC_p[a] J/g K	T_g, °C	ΔT, °C	ξ_a[b] nm	N_{CRR}[c]	d_{clay}, nm	ΔC_p[a] J/g K	T_g °C	ΔT, °C	ξ_a[b] nm	N_{CRR}[c]	d_{clay}, nm	
PTN	0.145	92	21	4.3	245	–	0.075	105	50	3.1	90	–	36
PTNC1	0.275	96	24	3.2	100	3.3	0.09	111	56	2.7	60	3	37
PTNC5	0.254	97	26	3.1	95	3.3	0.1	111	60	2.5	50	3	37
PTNC15	0.251	98	27	3.1	90	3.3	0.105	111	63	2.4	40	3	38
Clay						2.3						2.3	

[a] ΔC_p is normalized for the clay content.
[b] ξ_a values are limited to one digit after the decimal place.
[c] N_{CRR} values are rounded to nearest five.
[d] Crystallinity is determined using the expression; $X_c = \Delta H/\Delta H^0(1-\Phi)$, where Φ is the wt% of layered clay.

3.2. Effect of cold crystallization and drawing on the glass-transition dynamics

T_g reflects the cooperative relaxation of the polymer chains in the amorphous phase and has been sensitive to the structure of the system. Both crystallization and uniaxial drawing can modify the chain mobility which in turn alters T_g of the system. To probe the cold crystallization effect on T_g behavior, Fig. 7 shows the tan δ curves for the undrawn amorphous and crystallized samples of PTN and PTNC's. T_g is evaluated from the peak maximum of the tan δ curves. The peak width (ΔT) of the tan δ curves of PTN and PTNC's becomes wider after crystallization indicating the broader distribution of the relaxation rate. Additionally, the crystallized PTN and PTNC's contain a slight kink at the higher temperature side which may attribute to the rigid amorphous phase [62]. T_g of the undrawn amorphous (Fig. 7a) and crystallized PTNC's (Fig. 7b) decreases gradually up to 5 °C, compared to the neat PTN. Moreover, T_g of PTN and PTNC's shift up to 24 °C after the cold crystallization. Usually, crystallization causes the positive shift in T_g because of the geometric confinement induced by the crystallites which constraints the chain mobility in the amorphous phase [63]. Interestingly, regardless to the amorphous and crystallized structures, the incorporation of layered clay reduces T_g of the PTN matrix before drawing.

Fig. 8 shows the effect of drawing on the T_g behavior of PTN and PTNC's samples. T_g of the drawn amorphous (Fig. 8a) and crystallized PTNC's (Fig. 8b) increases steadily up to 6 °C, relative to the neat PTN. Whereas comparing the undrawn and drawn neat PTN, T_g reduces from 99 °C to 92 °C for amorphous structure and 123 °C to 105 °C for crystallized structure, respectively. Several studies of the bulk polymers under stress [64–66] manifested the decrease in T_g due to the increase in free volume. Surprisingly, drawn amorphous and crystallized PTNC's exhibit the positive shift in the sign of T_g, despite the fact that T_g decreases with the addition of layered clay in the neat PTN (Fig. 7) as well as after drawing. Notably, the crystallinity is almost similar within the experimental error for the

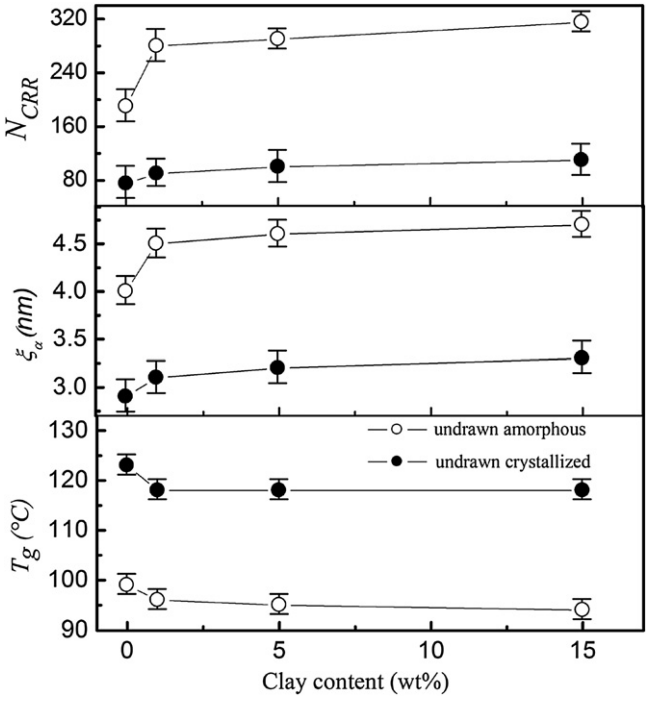

Fig. 9. The glass transition temperature (T_g), length scale of cooperativity (ξ_a) and the number of segments (N_{CRR}) of undrawn amorphous and crystallized structures of PTN and PTNC's as a function of clay content.

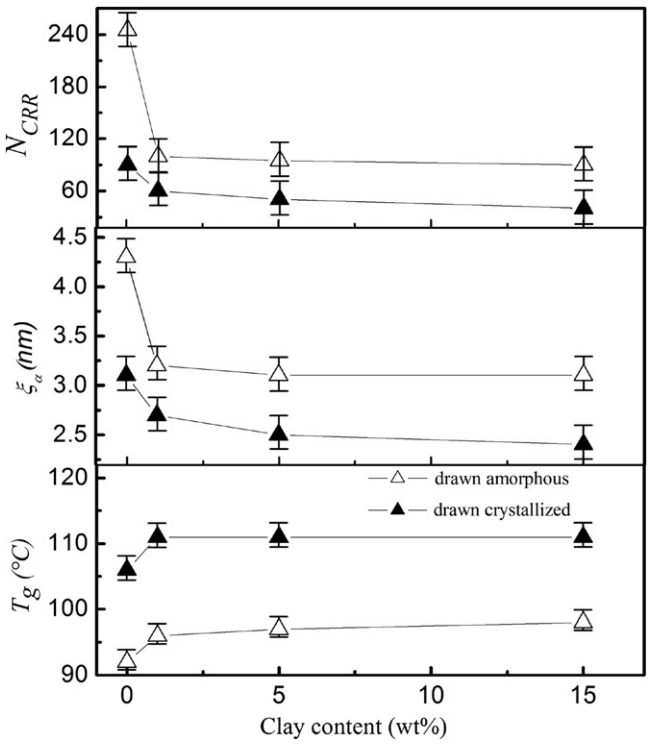

Fig. 10. The glass transition temperature (T_g), length scale of cooperativity (ξ_a) and the number of segments (N_{CRR}) of drawn amorphous and crystallized structures of PTN and PTNC's as a function of clay content.

undrawn and drawn crystallized PTNC's (Tables 1 and 2). Thus, the unusual increase in T_g of the drawn PTNC's may pertain to the formation of the house of cards type structure of the layered clay in the PTN matrix.

The shifting trend of T_g for PTNC's is further delineated through the determination of characteristic length (ξ_a) and the number of particles involved in a CRR (N_{CRR}) using Donth approach [49]. The parameters required for the calculation of CRR size are listed in Table 1 and Table 2 for the undrawn and drawn conditions, respectively. Fig. 9 shows the trend of deviation in T_g, ξ_a and N_{CRR} with respect to the clay content for the undrawn amorphous and crystallized PTNC's. Within the experimental error, T_g, ξ_a and N_{CRR} contain valid trend of variation. In both cases of the undrawn amorphous and crystallized PTNC's, the decrease of T_g compared to neat PTN render the increase in ξ_a and N_{CRR} values as a function of clay content. At 1 wt% of layered clay, there is a substantial rise in the ξ_a and N_{CRR} values with the corresponding drop in the T_g, whereas these values are slightly changed at higher clay content. Such rise in the ξ_a and N_{CRR} values indicates an enhanced cooperative mobility owing to the relative increase in the free volume by the incorporation of layered clay. Moreover, the ξ_a and N_{CRR} values are relatively smaller after the cold crystallization due to the geometric confinement of the amorphous phase.

Fig. 10 shows the shifting trend of T_g, ξ_a and N_{CRR} for the drawn amorphous and crystallized PTNC's with respect to the clay content. For the neat PTN, ξ_a and N_{CRR} values are slightly increased with the decrease in T_g after drawing. In the drawn amorphous and crystallized PTNC's, the increase of T_g compared to neat PTN causes the decrease in ξ_a and N_{CRR} values as a function of clay content. However, the ξ_a and N_{CRR} values are reduced considerably at 1 wt% of layered clay with the concomitant increase of T_g, whereas at higher clay content, further variation in these values is small. The decline in ξ_a and N_{CRR} values under drawing infers the retarded cooperative segmental mobility at T_g. Hence, the chain dynamics of PTN is strongly altered by the spatial arrangement of the layered clay in the system as found from Figs. 9 and 10. The randomly oriented clay platelets in the PTN matrix enhanced the chain mobility while the formation of the house of cards-like structure retarded the chain mobility. Moreover, the T_g, ξ_a and N_{CRR} values markedly vary at 1 wt% of the layered clay and then level off with the increasing clay content. This may correspond to the well dispersion of layered clay at lower content than at higher clay content while keeping the same intercalation extent (see the Tables for the values of intercalation).

Furthermore, the WAXD pattern of drawn amorphous PTN and PTNC5 is shown in Fig. 11, to characterize the orientational arrangement of the layered clay and PTN chains. The WAXD pattern of PTNC5 (Fig. 11a) exhibits the house of cards type structure of layered clay with the *c*-axis rotation, while the distinct (002) reflection in the meridional direction indicates the formation of nematic-like order of the PTN chains along the *c*-axis. Such nematic order is also observed in the neat amorphous PTN after drawing (Fig. 11b). The existence of nematic phase acts as a precursor for the orientation induced crystallization, reported for the quenched samples of PET [67]. However, in amorphous PTN, the presence of nematic phase also contributes to the evolution of free volume as evident from the decrease in T_g after drawing (Fig. 8). Thereby, despite the increase in the free volume, the unusual positive

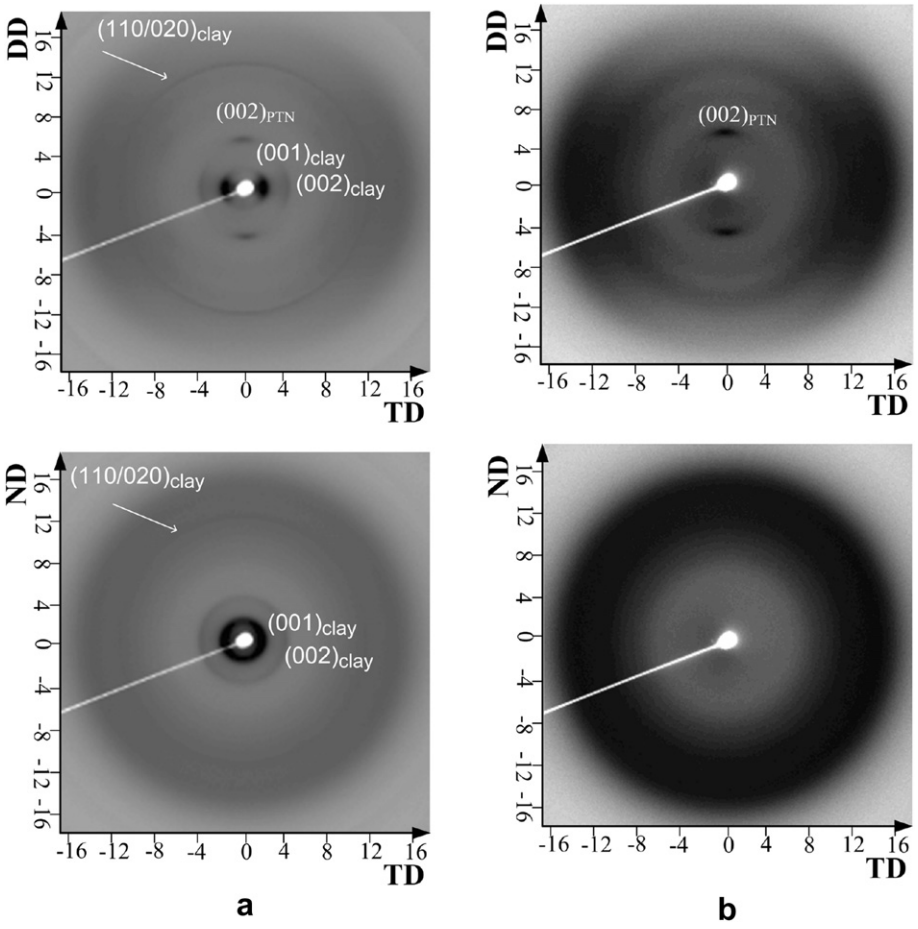

Fig. 11. WAXD pattern of the drawn amorphous structure of (a) PTNC5 and (b) neat PTN.

shifting trend of T_g in the drawn PTNC's may ascribe to the predominance of the conformational and surface effects among the layered clay and PTN chains.

Based on the structural illustration (Figs. 4–6, 11), the inclusion of layered clay in the PTN matrix leads to the development of two dominant effects; (i) intercalation of chains, and (ii) physical association/adsorption of chains to the clay surface, forming an interfacial region. The deviation in the sign of T_g is evaluated by the existence of finite size layer ξ_a as shown in Fig. 12. In case of the random dispersion of layered clay for undrawn amorphous

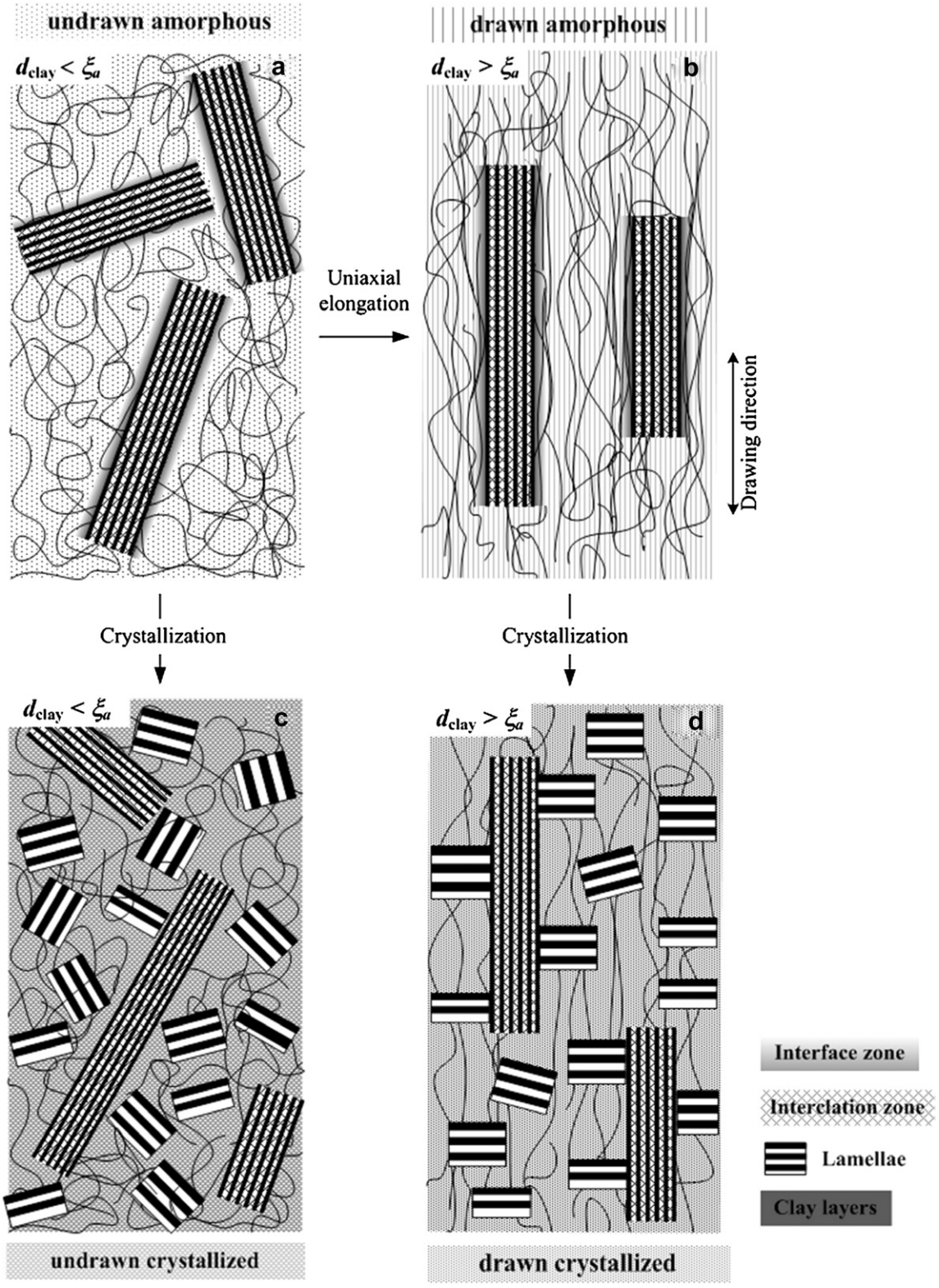

Fig. 12. The schematic illustration for the confinement effect of layered clay in the PTN matrix for the modification of the glass transition temperature (T_g) in the (a) undrawn amorphous, (b) drawn amorphous, (c) undrawn crystallized and (d) drawn crystallized conditions.

condition (Fig. 12a), the intergallery spacing is lower than the cooperative characteristic length ($d < \xi_a$) as a result the intercalated polymer chains exhibit the confinement effect. Under confinement, the polymer chains are mechanically aligned in the narrow spaces of the intergalleries, reducing the entanglement density relative to the neat PTN which increases the local free volume and consequently enhances the chain dynamics of the system. Moreover, the coil conformation of PTN chains in the interfacial region may contribute to further increase the local free volume at the interface. Whereas, taking into account the cold crystallization effect, geometric confinement is induced in the system (Fig. 12c), where incorporation of crystalline fraction reduces the amorphous fraction and hence lowers the free volume at the interface. But interlayer spacing is still lower than the CRR size ($d < \xi_a$) after the crystallization. Therefore, the free volume effect, arising from the confinement of the intercalated chains dominates and in turn causes to decrease T_g in the undrawn condition.

In case of the drawn condition (Fig. 12b and 12d), the intergallery spacing is larger than the CRR length ($d > \xi_a$), for which the confinement effect is not prevalent. Recently, Bandi et al. [12] revealed that the intercalated chains did not yield the confinement effect for $d > \xi_a$ and supports our assertion. However, drawing compels the polymer chains to be extended, forming the higher degree of nematic order at the clay surface for the amorphous PTNC's (Fig. 12b). Such mechanically extended chains are nearly flattened and the conformations are dramatically distorted in the interfacial region. In the meanwhile, the layered clay arranges like a house of cards type structure after drawing, imposing physical jamming to the clay layers and thereby constraints the mobility of the chains physically associated to the clay surface. Furthermore, the inducement of crystallinity under drawing (Fig. 12d) not only incorporates geometric confinement but also imposes physical jamming due to the arrangement of the house of cards like structure. As a ramification, the entropic constraint becomes dominant which retards the chain dynamics and ultimately raises T_g for the drawn condition.

4. Conclusion

The structure-properties relationships of PTN/layered clay nanocomposites are investigated under the drawing and cold crystallization effects. The uniaxial drawing of PTN and PTNC's cold-crystallized samples at 110 °C induces the α-crystal form with the chain axis (*c*-axis) aligned along the drawing direction as well as parallel to the layered clay surface. As a result, the broad surfaces of the clay platelets become nearly perpendicular to the sample's surface, exhibiting the house of cards like structure due to the specific orientational relationship between the α-crystal form and clay platelets. Probing the structural orientation effect on the T_g behavior reveals that the amorphous and crystallized structures exhibit the analogous tendencies in decreasing and increasing the T_g compared with the neat PTN before and after drawing, respectively. The relative shifting trend in T_g reflected by the variation of cooperative segmental mobility can be attributed to the random dispersion of layered clay before drawing and the development of house of cards-type structure after drawing. The unusual deviation in the sign of T_g for PTNC's (negative to positive shift) before and after drawing, is ascribed by the interplay of two competing effects; (i) the increase in the local free volume owing to the confining effect of intercalation, enhances the chain mobility and decreases T_g, (ii) the entropic constraints imposed by the stronger interfacial interaction due to the physical jamming of the layered clay after the formation of house of cards type structure, retards the chain mobility and raises T_g.

References

[1] Ray SS, Okamoto M. Prog Polym Sci 2003;28:1539.
[2] Winey KI, Vaia RA. MRS Bull 2007;32:214.
[3] Usuki A, Hasegawa N, Kato M. Adv Polym Sci 2005;179:135.
[4] Giannelis EP, Krishnamoorti R, Manias E. Adv Polym Sci 1999;138:107.
[5] Shah D, Maiti P, Jiang DD, Batt CA, Giannelis EP. Adv Mater 2005;17:525.
[6] Bousmina M. Macromolecules 2006;39:4259.
[7] Srivastava S, Basu JK. Phys Rev Lett 2007;98:165701.
[8] Hernandez MC, Suarez N, Martinez LA, Feijoo JL, Monaco SL, Salazar N. Phys Rev E 2008;77:051801.
[9] Arceo A, Meli L, Green PF. Nano Lett 2008;8:2271.
[10] Bansal A, Yang H, Li G, Cho K, Benicewicz BC, Kumar SK, et al. Nat Mater 2005;4:693.
[11] Narayanan RA, Thiyagarajan P, Lewis S, Bansal A, Schadler LS, Lurio LB. Phy Rev Lett 2006;97:075505.
[12] Bandi S, Schiraldi DA. Macromolecules 2006;39:6537.
[13] Rao Y, Pochan JM. Macromolecules 2007;40:290.
[14] Vyazovkin S, Dranca I. J Phys Chem B 2004;108:11981.
[15] Oh H, Green PF. Nat Mater 2009;8:139.
[16] Lu H, Nutt S. Macromolecules 2003;36:4010.
[17] Tran TA, Said S, Grohens Y. Macromolecules 2005;38:3867.
[18] Li Y, Ishida H. Macromolecules 2005;38:6513.
[19] Xia H, Song M. Thermochim Acta 2005;429:1.
[20] Alcoutlabi M, McKenna GB. J Phys Condens Matter 2005;17:R461.
[21] Priestley RD, Ellison CJ, Broadbelt LJ, Torkelson JM. Science 2005;309:456.
[22] Baschnagel J, Varnik F. J Phys Condens Matter 2005;17:R851.
[23] Kropka JM, Pryamitsyn V, Ganesan V. Phys Rev Lett 2008;101:075702.
[24] Bohning M, Goering H, Fritz A, Brzezinka KW, Turky G, Schonhals A, et al. Macromolecules 2005;38:2764.
[25] Tsui OKC, Russell TP, Hawker CJ. Macromolecules 2001;34:5535.
[26] Kuppa V, Foley TMD, Manias E. Eur Phys J E 2003;12:159.
[27] Tran TA, Said S, Grohens Y. Compos Part A Appl Sci 2005;36:461.
[28] Chen K, Wilkie CA, Vyazovkin S. J Phys Chem B 2007;111:12685.
[29] Vaia RA, Sauer BB, Tse OK, Giannelis EP. J Polym Sci Part B Polym Phys 1997;35:59.
[30] Donth E. The glass transition, relaxation dynamics in liquids and disordered materials, springer series in materials science, vol. 48. New York: Springer; 2001.
[31] Anastasiadis SH, Karatasos K, Vlachos G. Phys Rev Lett 2000;84:915.
[32] Jerome BJ. Phys Condens Matter 1999;11:A189.
[33] de Gennes PG. Eur Phys J E 2000;2:201.
[34] Brown HR, Russell TP. Macromolecules 1996;29:798.
[35] Ash BJ, Siegel RW, Schadler LS. J Polym Sci Part B Polym Phys 2004;42:4371.
[36] Baljon ARC, Billen J, Khare R. Phys Rev Lett 2004;93:255701.
[37] O'Connell PA, McKenna GB. Science 2005;307:1760.
[38] Balazs AC, Emrick T, Russell TP. Science 2006;314:1107.
[39] Rittigstein P, Torkelson JM. J Polym Sci Part B Polym Phys 2006;44:2935.
[40] Jeong YG, Jo WH, Lee SC. Polymer 2004;45:379;
Jeong YG, Jo WH, Lee SC. Polymer 2003;44:3259.
[41] Liang Y, Lee HS. Macromolecules 2005;38:9885.
[42] Liang Y, Zheng M, Park KH, Lee HS. Polymer 1961;2008:49.
[43] Chuang WT, Hong PD, Chen CH, Sheu HS, Jeng US. J Appl Cryst 2007;40:s637.
[44] Stier U, Schawaller D, Oppermann W. Polymer 2001;42:8753.
[45] Stier U, Oppermann W. J Polym Sci Part A Polym Chem 2001;39:620.
[46] Product bulletin/cloisite@93A. Southern Clay Products, Inc.: TX (www.scprod.com/product_bulletins/PB%93ACloisite%9393A.pdf)
[47] Khan AN, Hong PD, Chuang WT, Shih KS. Mater Chem Phys 2010;119:93.
[48] Adam G, Gibbs JH. J Chem Phys 1965;43:139.
[49] Donth E. J Polym Sci Part B Polym Phys 1996;34:2881;
Donth E. J Non-Cryst Solids 1982;53:325.
[50] Kawakami D, Burger C, Ran S, Avila-Orta C, Sics I, Chu B, et al. Macromolecules 2008;41:2859.
[51] Kojima Y, Usuki A, Kawasumi M, Okada A, Kurauchi T, Kamigaito O, et al. J Polym Sci Part B Polym Phys 1995;33:1039.
[52] Schmidt G, Nakatani AI, Butler PD, Karim A, Han CC. Macromolecules 2002;35:4725.
[53] Bafina A, Beaucage G, Mirabella F, Mehta S. Polymer 2003;44:1103.
[54] Park SY, Cho YH, Vaia RA. Macromolecules 2005;38:1729.
[55] Wang K, Zhao P, Yang H, Liang S, Zhang Q, Du R, et al. Polymer 2006;47:7103.
[56] Fujiyama-Novak JH, Cakmak M. Macromolecules 2008;41:6444.
[57] Okamoto M, Nam PH, Maiti P, Kotaka T, Hasegawa N, Usuki A. Nano Lett 2001;1:295.
[58] Judge JT, Stein RS. J Appl Phys 1961;32:2357.
[59] Zhao Y, Keroach D, Prud-homme R. Marcomolecules 1999;32:1218.
[60] Park JW, Doi Y, Iwata T. Marcomolecules 2005;38:2345.
[61] Lincoln DM, Vaia RA, Wang ZG, Hsiao BS, Krishnamoorti R. Polymer 2001;42:9975.
[62] Arrighi V, McEsen IJ, Qiran H, Prieto MBS. Polymer 2003;44:6259.
[63] Cheng SZ, Wu ZQ, Wunderlich B. Macromolecules 1987;20:2802.
[64] Turnbull D, Cohen MH. J Chem Phys 1961;34:120;
Turnbull D, Cohen MH. J Chem Phys 1970;52:3038.
[65] Chow TS. Polym Eng Sci 1984;24:915.
[66] Loo L, Choen R, Gleason K. Science 2000;288:116.
[67] Reiter G, Strobl GR, editors. Progress in understanding of polymer crystallization. Berlin Heidelberg: Springer; 2007 [chapter 6].